PEIE: Physics Embedded Illumination Estimation for Adaptive Dehazing

Huaizhuo Liu[1,2,3], **Hai-Miao Hu**[1,2,3*], **Yonglong Jiang**[3], **Yurui Liu**[1,2,3]

[1]Hangzhou Innovation Institute, Beihang University
[2]State Key Laboratory of Virtual Reality Technology and Systems, Beihang University
[3]School of Computer Science and Engineering, Beihang University
{lhz549, hu}@buaa.edu.cn

Abstract

Deep learning-based methods have made significant progress in image dehazing. However, these methods often falter when applied to real-world hazy images, primarily due to the scarcity of paired real-world data and the limitations of current dehazing feature extractors. Toward these issues, we introduce a novel Physics Embedded Illumination Estimation (PEIE) method for adaptive real-world dehazing. Specifically, (1) we identify the limitations of the widely used Atmospheric Scattering Model and propose a new physical model, the Illumination-Adaptive Scattering Model (IASM), for more accurate illumination representation in hazy imaging; (2) we develop a robust data synthesis pipeline that leverages the physics embedded illumination estimation to generate realistic hazy images; and (3) we design an Illumination-Adaptive Dehazing Unit (IDU) to extract dehazing features consistent with our proposed IASM in the latent space. By integrating the IDU into a U-Net architecture to create IAD-Net, we achieve significant improvements in dehazing performance through end-to-end training on synthetic data. Extensive experiments validate the superior performance of our PEIE method, significantly surpassing the state-of-the-arts in real-world dehazing.

Introduction

Haze is a common natural phenomenon that significantly degrades image quality, impairing human visual perception and adversely impacting high-level vision tasks (Liao et al. 2023; Zhou et al. 2023; Li et al. 2023). Consequently, numerous studies have sought to develop effective dehazing techniques to restore clean images from hazy inputs. According to the Atmospheric Scattering Model (ASM) (Narasimhan and Nayar 2002, 2003), the hazing process is typically formulated as:

$$\mathbf{I}(\mathbf{x}) = \mathbf{J}(\mathbf{x})t(\mathbf{x}) + \mathbf{A}(1 - t(\mathbf{x})) \tag{1}$$

where $\mathbf{x}$ denotes the pixel coordinate, $\mathbf{I}$ represents the observed hazy image, $\mathbf{J}$ is the clean image to be restored, $\mathbf{A}$ is the global atmospheric light, and t is the transmission map. Under the assumption of a homogeneous atmosphere, t can be expressed as $t(\mathbf{x}) = e^{-\beta d(\mathbf{x})}$, where β is the scattering coefficient and d is the scene depth.

*Corresponding Author.

(a) Hazy (b) PSD (c) RIDCP (d) Ours

Figure 1: Dehazing results on a real hazy image.

The ASM suggests that single image dehazing is an ill-posed problem without precise knowledge of $\mathbf{A}$ and t. Early methods (He, Sun, and Tang 2011; Meng et al. 2013; Fattal 2015; Berman, Treibitz, and Avidan 2016; Bui and Kim 2018; Ling et al. 2023) typically estimate t using hand-crafted priors, identify the most haze-opaque region for $\mathbf{A}$, and then restore the clean image based on the ASM. However, these priors are not always reliable, resulting in suboptimal dehazing results.

The advent of deep learning has significantly advanced dehazing. Many methods leverage ASM-inspired architectures (Cai et al. 2016; Ren et al. 2016; Li et al. 2017; Yang, Xu, and Luo 2018; Zhang and Patel 2018; Dong and Pan 2020; Zheng et al. 2023), while others adopt end-to-end designs without explicit physical modeling (Qin et al. 2020; Dong et al. 2020; Guo et al. 2022; Qiu et al. 2023; Wang et al. 2024a; Zhang, Zhou, and Li 2024; Wang et al. 2024c). These approaches are typically trained on synthetic data generated using ASM (Li et al. 2019). However, the domain gap between synthetic and real-world images often limits their generalization to real-world hazy scenes.

Recent research has increasingly focused on addressing this problem. Some studies adopt semi-supervised (Li et al. 2020; Shao et al. 2020; Liu et al. 2021; Chen et al. 2021)

or unsupervised (Yang et al. 2022; Wang et al. 2024b) approaches to reduce reliance on paired data. Others attempt to generate more realistic paired data (Gong et al. 2021; Li et al. 2022; Wu et al. 2023; Fan et al. 2024) to bridge the domain gap. Despite these advancements, there remains considerable potential for further improvement, particularly in terms of the realism of the synthetic data.

In this paper, we propose a novel Physics Embedded Illumination Estimation (PEIE) method for real-world adaptive dehazing. We begin by analyzing the limitations of the ASM, particularly its inability to accurately model complex illumination scenes, such as non-uniform illumination or glow from multiple scattering. These shortcomings lead to issues like the generation of unrealistic synthetic data and the design of less effective networks. To address these limitations, we propose a new physical model called the Illumination-Adaptive Scattering Model (IASM), which provides a more accurate representation of hazy images under diverse illumination conditions. Building on the IASM, we introduce an advanced haze synthesis pipeline that leverages the physics embedded illumination estimation to generate more realistic hazy images for network training. Furthermore, We design an Illumination-Adaptive Dehazing Unit (IDU), which extracts dehazing features consistent with the physical model in latent space by considering the physical characteristics of each parameter and their interactions. By integrating the IDU into a U-Net architecture, we construct the Illumination-Adaptive Dehazing Network (IADNet).

As demonstrated in Figure 1, our PEIE produces superior dehazing and exposure results compared to state-of-the-art real-world dehazing methods, such as PSD (Chen et al. 2021) and RIDCP (Wu et al. 2023). Our key contributions are summarized as follows:

- We propose a novel physical model, the Illumination-Adaptive Scattering Model (IASM), which extends the ASM to describe real hazy scenes under varying illumination conditions more accurately.
- Leveraging the IASM, we develop a data synthesis pipeline based on the proposed physics embedded illumination estimation method, which generates high-quality hazy-clean image pairs to bridge the domain gap. Additionally, we design the Illumination-Adaptive Dehazing Unit (IDU) to more effectively capture dehazing features within the latent space, which is integrated into our Illumination-Adaptive Dehazing Network (IADNet). To our best knowledge, this is the first attempt to achieve these advancements using an improved physical model.
- We compared our method with state-of-the-art methods through comprehensive experiments. Both subjective evaluations and no-reference quality metrics demonstrate that PEIE achieves superior dehazing performance and robust adaptation to diverse illumination conditions.

Related Work

Single image dehazing. The Atmospheric Scattering Model (ASM), as defined in Eq.(1), presents a highly ill-posed problem in the context of single image dehazing. Early approaches attempted to mitigate this issue by introducing statistical priors based on the characteristics of clean images (He, Sun, and Tang 2011; Meng et al. 2013; Fattal 2015; Berman, Treibitz, and Avidan 2016; Bui and Kim 2018; Ling et al. 2023), thereby making the problem more tractable. Although these handcrafted priors have shown effectiveness in various scenarios, they often struggle with specific cases, such as sky regions or areas with homogeneous color, where transmission estimates can become inaccurate. Consequently, these methods may not be universally effective across all types of hazy images.

With the advent of deep learning, data-driven methods for haze removal have gained substantial traction. Early methods (Cai et al. 2016; Ren et al. 2016; Yang, Xu, and Luo 2018; Zhang and Patel 2018) primarily focused on estimating the parameters of the ASM in Eq.(1). However, these methods are prone to cumulative errors due to the need to estimate multiple parameters simultaneously. To overcome this limitation, researchers have developed end-to-end networks that either re-customize the ASM (Li et al. 2017), incorporate it within the latent space (Dong and Pan 2020; Zheng et al. 2023), or design networks that operate independently of the physical model altogether (Qin et al. 2020; Dong et al. 2020; Guo et al. 2022; Qiu et al. 2023; Wang et al. 2024a; Zhang, Zhou, and Li 2024; Wang et al. 2024c). While these methods have demonstrated impressive performance on synthetic datasets, they often face significant challenges when applied to real-world images, primarily due to the domain gap between synthetic and real data.

In recent years, there has been a growing focus on addressing the challenges associated with real-world dehazing. Some approaches have sought to reduce dependency on paired real data by introducing specialized loss functions (Li et al. 2020; Chen et al. 2021) or employing cycle consistency designs (Shao et al. 2020; Yang et al. 2022) to facilitate semi-supervised or unsupervised training. Another promising direction involves the generation of more realistic paired data to guide the training process (Gong et al. 2021; Li et al. 2022; Wu et al. 2023; Fan et al. 2024). Despite these advancements, significant challenges remain, particularly in adapting to varying illumination conditions. Our study addresses these issues by proposing a more robust physical model that guides the synthesis of more realistic hazy-clean pairs, leading to improved dehazing results.

Degradation models. Several studies have identified limitations in the ASM and have proposed various improvements. (Li, Tan, and Brown 2015) suggested that the primary source of light in night haze imaging comes from various active light sources, arguing that using global atmospheric light leads to inaccuracies. (Hu et al. 2019, 2020) extended this approach to daytime scenes to address issues of non-uniform illumination and glow effects. (Ju et al. 2021) emphasized that incident illumination affects scenes differently, as light can be trapped in textures, with absorption rates varying based on texture density. While these models offer more accurate representations, they typically focus on either the first or second term of the scattering model. In contrast, our IASM addresses issues in both terms of the ASM and

introduces a simple yet effective modification for more accurate modeling.

Observation and Justification

In this section, we discuss our observations and provide justifications for the limitations of the widely used Atmospheric Scattering Model (ASM), as described in Eq. (1).

The ASM comprises two main components: the first term, attenuation, describes how scene reflection reaches the camera after scattering, while the second term, airlight, represents environmental illumination scattered toward the observer, effectively turning the atmosphere into a light source. This model is popular in dehazing methods due to its simplicity and effectiveness.

In the first term, the clean image $\mathbf{J}$ is often expressed as $\mathbf{AR}$ (Narasimhan and Nayar 2003), where $\mathbf{R}$ denotes the reflectance of scene points, and $\mathbf{A}$ represents the incident illumination, as illustrated in Figure 2. This formulation assumes that the incident illumination across the scene is primarily determined by atmospheric light, with contributions from other light sources considered negligible. Some methods attempt to restore $\mathbf{J}$ directly, but this approach can lead to dim results, especially in regions with low incident illumination, as shown in Figure 3(b). Other methods focus on restoring $\mathbf{R}$, which can result in over-saturation in certain image regions due to the global constant nature of $\mathbf{A}$, which fails to capture the actual distribution of incident illumination, as seen in Figure 3(c).

In the second term, $\mathbf{A}$ represents environmental illumination from sources such as direct sunlight, diffuse skylight, and light reflected by the scene, as shown in Figure 2. While this assumption generally holds due to the consistency of these light sources across the scene, it becomes inadequate under adverse weather conditions or in the presence of active light sources. In such cases, phenomena like the glow effect caused by multiple scattering in bad weather and light emitted by active sources lead to non-uniform environmental illumination. These glow effects, characterized by localized intensity variations, typically occur near the sky or around active light sources, as shown in Figure 3(e), and result in artifacts in the final dehazed image, as seen in Figure 3(f).

Based on these observations regarding the limitations of the ASM, we propose a Physics Embedded Illumination Estimation (PEIE) method for real-world adaptive dehazing, which is well-suited for haze images with varying haze concentrations and illumination conditions.

Proposed Method

In this section, we introduce our Physical Embedded Illumination Estimation (PEIE) method for real-world adaptive dehazing. The overall framework of the proposed method is illustrated in Figure 4. Given an input image, we first estimate varying illuminations through physical embedding and synthesize a corresponding hazy image. This hazy image is then processed by IADNet, a dehazing network built by physics, to get the corresponding restored image.

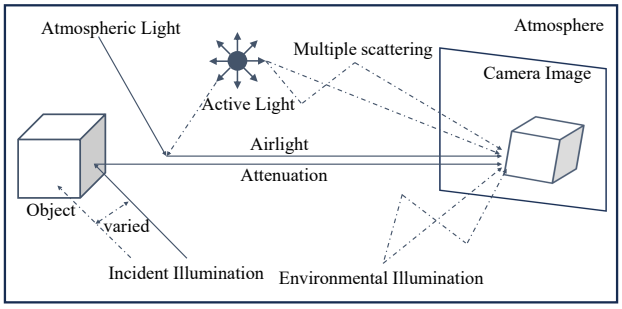

Figure 2: Diagram illustrating the hazy imaging process. The solid line represents the range modeled by ASM, while the dotted line indicates the range beyond ASM's capability.

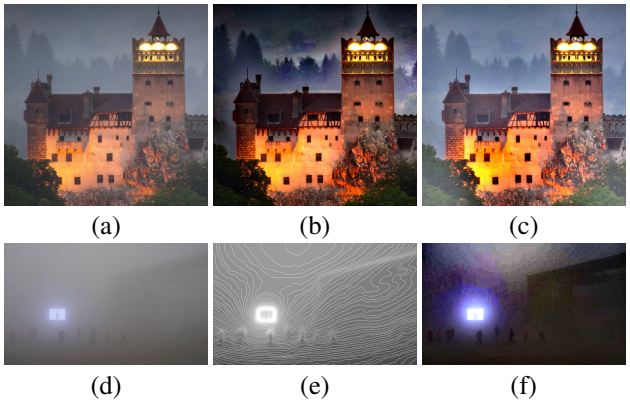

Figure 3: Failure cases of ASM. (a) and (d) are two real hazy images. (b) and (c) are the results of processing (a) using SLP and IDE, respectively. (e) displays the contour map of (d), and (f) shows the result of processing (d) using SLP.

Illumination-Adaptive Scattering Model

To address the shortcomings of the ASM, we introduce the Illumination-Adaptive Scattering Model (IASM), which serves as the physical cornerstone of our PEIE method.

In contrast to the ASM, which uses a global constant $\mathbf{A}$ in the first term, our model introduces local incident illumination $\mathbf{L_I}$ to more accurately represent the varying light intensity at different scene points. This adjustment allows for a more precise restoration of the scene reflectance $\mathbf{R}$. Additionally, we replace the global constant $\mathbf{A}$ in the second term with local environmental illumination $\mathbf{L_E}$. Unlike ASM, which assumes uniform environmental illumination across the scene, our model accounts for variations throughout the 3D space. To manage this complexity, we approximate the cumulative scattering effects along the path from the scene point to the observer as a combination of scattering from a series of identical sources, effectively reducing the problem to a 2D variation. The complete model is expressed as:

$$\mathbf{I}(\mathbf{x}) = \mathbf{L_I}(\mathbf{x})\mathbf{R}(\mathbf{x})t(\mathbf{x}) + \mathbf{L_E}(\mathbf{x})(1 - t(\mathbf{x})) \qquad (2)$$

By introducing these local parameters, our IASM more accurately captures the true incident and environmental illu-

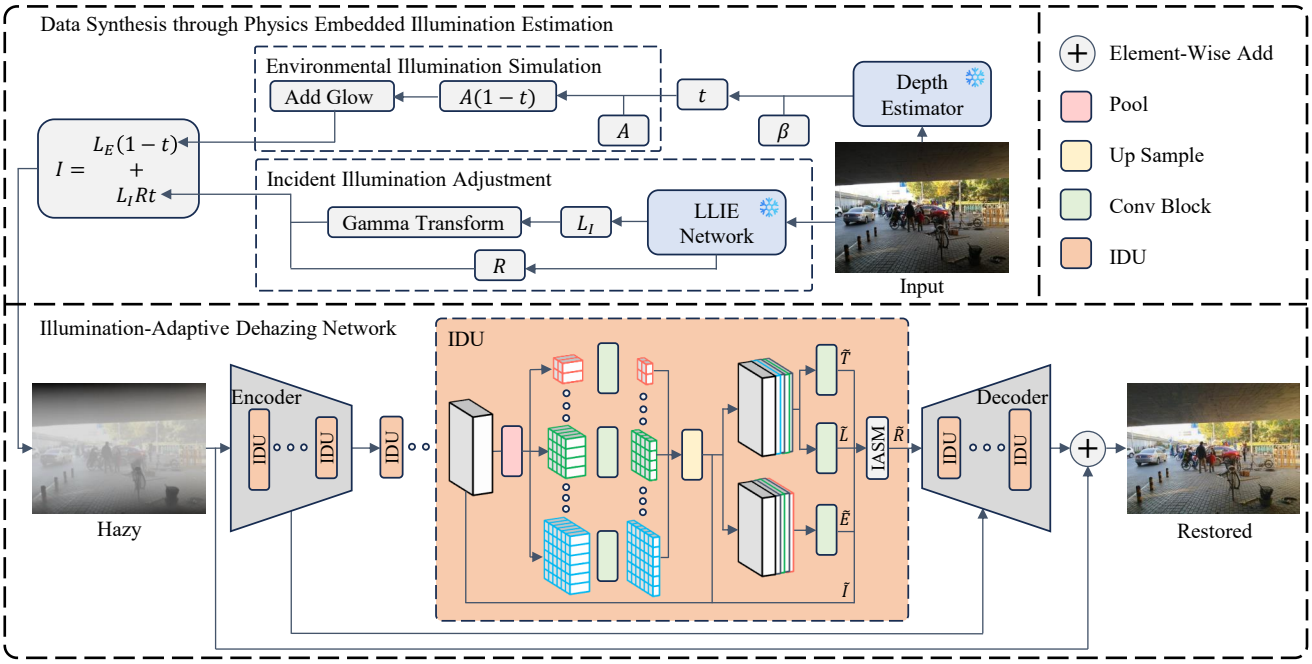

Figure 4: Overview of the PEIE. The upper part illustrates the dual-branch physical embedding illumination estimation method guiding data synthesis for a given input image. The lower part depicts IADNet, a U-Net architecture where standard convolutional blocks are replaced with the Illumination-Adaptive Dehazing Unit (IDU), designed under the guidance of IASM.

mination distributions, leading to improved dehazing results, as illustrated in Figure 1(d).

We further analyze the physical characteristics of these newly introduced parameters. Both $\mathbf{L_I}$ and $\mathbf{L_E}$ exhibit a degree of local smoothness, but incident illumination $\mathbf{L_I}$ shows more spatial variation due to factors such as material properties, incident angles, and occlusions, contributing to its fine-scale variation. In contrast, environmental illumination $\mathbf{L_E}$ is less affected by these factors, and its consistency is further enhanced by multiple scattering, leading to smoother variations over larger areas. Ablation experiments confirm this distinction in local consistency.

Our physics model differs significantly from previous efforts. While earlier models modified the first term to mitigate uneven incident illumination (Ju et al. 2021), adjusted the second term to capture non-uniform environmental illumination better (Hu et al. 2020), or introduced an additional term to model glow effects (Li, Tan, and Brown 2015; Hu et al. 2020). In contrast, our model simultaneously addresses non-uniform incident and environmental illumination using two local variables without the need for an additional term to model glow, thereby significantly enhancing the model's representational capacity.

Data Synthesis through Physics Embedded Illumination Estimation

Synthesizing more realistic degraded images is a well-established approach for improving real-world image restoration tasks (Wang et al. 2021a,b; Zhang et al. 2021; Wu et al. 2023). Since our proposed IASM offers a more accurate representation of the haze imaging process, we utilize it to synthesize haze images, as shown in the upper part of Figure 4. The synthesis process involves adjusting incident illumination and simulating environmental illumination in a physics-embedded dual-branch manner, as detailed below:

Incident Illumination Adjustment. To simulate incident illumination of varying intensities, we first extract the incident illumination from the input haze-free image, in alignment with the Retinex theory of brightness enhancement. We utilize Retinexformer (Cai et al. 2023) as a fixed low-light image enhancement(LLIE) module due to its robust capabilities. This allows us to obtain a clean reflectance image $\mathbf{R}$ from the input image, which then helps derive the incident illumination $\mathbf{L_I}$. The obtained reflectance image $\mathbf{R}$ also serves as a reference for supervised training.

For the extracted incident illumination, we apply a gamma transform to control its intensity and then multiply it with $\mathbf{R}$ to generate haze-free images under different illumination conditions. Unlike the RIDCP (Wu et al. 2023) method, which directly applies a gamma transform to the haze-free image, our approach first extracts the incident illumination. This step captures uneven illumination conditions, allowing us to enhance or diminish the illumination without making the entire image too dark, thereby more accurately simulating real-world illumination scenarios.

Environmental Illumination Simulation. While IASM effectively models environmental illumination, directly generating reasonable environmental illumination through random means is extremely challenging. Drawing inspiration

from (Hu et al. 2019), we simulate the full second term in IASM, representing scattering caused by environmental illumination. Specifically, we decompose this term into two parts: atmospheric light scattering $\mathbf{A}(1-t)$, representing haze caused by single scattering, and the glow term, which accounts for multiple scattering effects. For $\mathbf{A}$, we randomly generate values within the range $[0.8, 1.0]$. To approximate the glow term, which results from multiple scattering and produces a blur effect, we simulate it by applying a blur operation to the synthesized image as a whole.

Transmission is another key factor in data synthesis. We follow the previous methods, using a fixed depth estimation network (Yang et al. 2024) to get the depth map d and randomly generating $\beta \in [0.8, 2]$ to control haze density.

Although our improved data synthesis process enhances the realism of the generated images, it cannot fully encompass the entire degradation space observed in real-world scenarios. However, by refining the data synthesis approach, our method expands the solvable degradation boundary, improving upon previous methods in addressing real-world dehazing challenges.

Illumination-Adaptive Dehazing Network

Given the accuracy of our proposed IASM in modeling hazy images, we leverage it to design a more effective network architecture. However, directly estimating unknown factors in the original space can lead to cumulative errors, and the absence of real data for $\mathbf{L_E}$ complicates training.

To overcome these challenges, we turn to the latent space for guidance. Inspired by FDU (Dong and Pan 2020) and PDU (Zheng et al. 2023), we propose the Illumination-Adaptive Dehazing Unit (IDU) by applying IASM in the latent space. This approach enhances the interpretability of the dehazing process without requiring explicit ground truth for $\mathbf{L_E}$, as shown in Figure 4.

First, we derive a latent space representation of IASM, expressed in Eq. (3), through a series of algebraic transformations. In this representation, $\widetilde{\boldsymbol{I}}, \widetilde{\boldsymbol{R}}, \widetilde{\boldsymbol{E}}, \widetilde{\boldsymbol{L}}, \widetilde{\boldsymbol{T}}$ correspond to the latent representations of $\mathbf{I}, \mathbf{R}, \mathbf{L_E}, \mathbf{L_I}, t$ respectively, with $\odot$ denoting the Hadamard product.

$$\widetilde{\boldsymbol{R}} = \widetilde{\boldsymbol{I}} \odot (\widetilde{\boldsymbol{L}} \odot \widetilde{\boldsymbol{T}}) + \widetilde{\boldsymbol{E}} \odot (\widetilde{\boldsymbol{L}} - \widetilde{\boldsymbol{L}} \odot \widetilde{\boldsymbol{T}}), \tag{3}$$

We then explicitly construct the IDU using Eq.(3). To achieve this, we estimate the three unknown parameters from $\widetilde{\boldsymbol{I}}$ and then apply Eq.(3) to obtain the result. As discussed earlier, $\mathbf{L_E}$ and $\mathbf{L_I}$ exhibit local smoothness at different scales. Therefore, we extract features at varying scales for their respective latent representations, $\widetilde{\boldsymbol{E}}$ and $\widetilde{\boldsymbol{L}}$. Inspired by pyramid pooling (Zhao et al. 2017), we first apply pooling operations at N different scales to obtain multi-scale features, which are subsequently compressed into a single channel. These low-dimensional feature maps are then upsampled via bilinear interpolation to match the original feature map's size. To estimate $\widetilde{\boldsymbol{L}}$, we use the $N-1$ finer-scale features (*i.e.*, those derived using smaller pooling kernels) and concatenate them with $\widetilde{\boldsymbol{I}}$. This approach enables the capture of detailed information related to $\mathbf{L_I}$, which reflects local variations in incident light intensity. For estimating $\widetilde{\boldsymbol{T}}$, which correlates with depth and also exhibits fine local smoothness, we use the same set of finer-scale features. In contrast, $\widetilde{\boldsymbol{E}}$ is estimated using the $N-1$ coarser-scale features, which provide a broader contextual understanding, making them better suited for capturing environmental illumination variations associated with $\mathbf{L_E}$. With the proposed IASM, interpretable features $\widetilde{\boldsymbol{R}}$ can be generated from the input features $\widetilde{\boldsymbol{I}}$ for restoring hazy images.

Building on the proposed IDU, we develop our IADNet, illustrated in Figure 4. IADNet is based on a U-Net-like backbone but includes several key modifications: 1) We replace convolutional layers with our IDU for enhanced dehazing feature extraction. 2) We add a global residual connection to simplify training.

Experiments

Implementation Details

We utilize 500 clean images from RIDCP (Wu et al. 2023) as input in our data synthesis pipeline, guiding network training through online synthesis. In the IDU, we employ average pooling layers with sizes $[4, 8, 12, 16, 24]$, where the size scales with the feature map size. Training is conducted using the Adam optimizer with default parameters ($\beta_1 = 0.9$, $\beta_2 = 0.99$), a fixed learning rate of 1×10^{-4}, and a batch size of 16. Data augmentation includes random resizing and cropping to 256 × 256, flipping with a 50 percent probability, and the addition of noise. Our proposed IADNet is trained on data generated by the synthesis pipeline over 10,000 iterations. We utilize L1 loss, perceptual loss, and GAN loss which are widely used in image restoration as objective functions, with weights of 1.0, 1.0, and 0.1, respectively. All experiments are implemented using the PyTorch framework on 4 NVIDIA RTX 2080Ti GPUs. More details can be found at https://github.com/Hankitle/PEIE.

Comparisons with SOTAs

We compare PEIE with several state-of-the-art methods: IDE (Ju et al. 2021), SLP (Ling et al. 2023), DAD (Shao et al. 2020), PSD (Chen et al. 2021), D4 (Yang et al. 2022), and RIDCP (Wu et al. 2023). SLP and IDE are traditional methods based on the ASM (ASM) and an enhanced physical model, respectively. The other four methods employ deep learning for real-world dehazing. Our evaluation includes visual quality comparison, no-reference image quality metrics, and human subjective study.

Visual Quality Comparison. We first assess the visual quality of PEIE on real hazy images from the RTTS subset of the RESIDE dataset (Li et al. 2019), which contains 4,322 real-world hazy images. The results are presented in Figure 5. To further demonstrate PEIE's superior generalization ability, we also evaluate it on Fattal's dataset (Fattal 2015), which includes 31 classic real hazy cases. The corresponding results are shown in Figure 6. From Figure 5 and Figure 6, we observe that while IDE and PSD achieve good exposure, they sometimes result in over-saturation. SLP and D4 tend to darken the images and introduce artifacts, especially

(a) Hazy (b) IDE (c) SLP (d) DAD (e) PSD (f) D4 (g) RIDCP (h) Ours

Figure 5: Comparison of dehazing results on real hazy images from RTTS. Zoom in for the best view.

(a) Hazy (b) IDE (c) SLP (d) DAD (e) PSD (f) D4 (g) RIDCP (h) Ours

Figure 6: Comparison of dehazing results on real real hazy images from Fattal's. Zoom in for the best view.

noticeable in the sky area. DAD and RIDCP produce effective dehazing, but they occasionally cause color distortion. In contrast, PEIE consistently generates high-quality, haze-free images with improved brightness and enhanced detail.

No-Reference Image Quality Assessment. Due to the lack of ground-truth reference images for real hazy scenes, our quantitative evaluation relies on no-reference image quality indices. Specifically, we employ FADE (Choi, You, and Bovik 2015) to assess haze density, along with three other metrics: NIQE (Mittal, Soundararajan, and Bovik 2013), BRISQUE (Mittal, Moorthy, and Bovik 2012), and NIMA (Talebi and Milanfar 2018), all evaluated on the RTTS dataset as shown in Table 1. NIQE and BRISQUE, which measure overall image quality, indicate that PEIE achieves the highest scores among the methods compared. NIMA, which predicts aesthetic quality, ranks PEIE second only to RIDCP, reflecting that PEIE's dehazing results are both clean and visually appealing. Although PEIE ranks third in FADE, this metric tends to favor darker images, leading to higher scores for methods like D4 and SLP, as shown in Figure 5. In contrast, PEIE enhances image brightness while maintaining competitive FADE scores. Overall, PEIE excels across all evaluated metrics, demonstrating its effectiveness for real-world dehazing tasks.

Human Subjective Study. We conducted a human subjective study to compare PEIE's performance with other methods using 10 real-world hazy images from the HSTS subset of RESIDE, specifically designed for subjective evaluation. Participants were instructed to select images that appeared cleaner, more visually pleasing, and featured high-quality details without color shifting. The images were displayed group by group, each containing the input image and results from different methods. Observers rated the restoration quality from 1 to 5. The evaluation scores in Table 1

Method	FADE↓	NIQE↓	BRISQUE↓	NIMA↑	HS↑
Hazy	2.484	5.214	36.642	4.573	-
IDE	1.007	4.148	29.558	4.618	3.66
SLP	0.916	4.352	30.515	4.665	3.47
DAD	1.451	5.364	34.553	4.488	3.87
PSD	0.998	3.807	20.432	4.325	3.96
D4	**0.893**	4.521	28.101	4.797	2.95
RIDCP	0.992	4.337	15.137	**4.919**	4.02
Ours	0.950	**3.753**	**11.762**	4.856	**4.36**

Table 1: Quantitative comparison on RTTS and human subjective study on HSTS. Bold and underline indicate the best and second-best, respectively.

Model	Data	NIQE↓	BRISQUE↓	NIMA↑
FFANet	OTS	4.979	34.372	4.594
	RIDCP	4.362	19.548	4.913
	PEIE	3.965	13.569	4.742
C2PNet	OTS	4.962	34.125	4.606
	RIDCP	4.455	17.192	4.882
	PEIE	4.347	12.814	4.810
DehazeFormer	OTS	4.835	28.268	4.614
	RIDCP	4.365	19.518	4.821
	PEIE	**3.719**	13.357	4.599
IADNet	OTS	4.962	33.844	4.598
	RIDCP	4.020	17.236	**4.967**
	PEIE	3.753	**11.762**	4.856

Table 2: Effectiveness of the data synthesis pipeline.

indicate that PEIE achieved the highest score, demonstrating its superior generalization performance.

Ablation Studies

We conduct several ablation experiments on RTTS to evaluate the effectiveness of key components in our method.

Effectiveness of the data synthesis pipeline. To evaluate the overall impact of the proposed data synthesis pipeline, we compare it with two alternatives: OTS (Li et al. 2019) and RIDCP (Wu et al. 2023). For a fair comparison, all pipelines use the same inputs and depth estimation method (Yang et al. 2024). Additionally, we train FFANet (Qin et al. 2020), C2PNet (Zheng et al. 2023) and DehazeFormer (Song et al. 2023) using these pipelines. The results are presented in Table 2, which indicate that networks trained with OTS and RIDCP face challenges in haze removal and exposure balance. By training with our pipeline, these networks achieve notable performance improvements. Among them, IADNet shows the most significant enhancement, achieving superior results across metrics compared to the other networks. These findings highlight the critical role of IASM, which serves as the core component of the proposed data synthesis pipeline and IADNet.

Contribution of specific data synthesis components. To assess the contribution of each component in the proposed data synthesis pipeline, we conduct ablation studies on both incident illumination adjustment and environmental illumination simulation. The results, presented in Table 3, highlight the contribution of each subcomponent to the overall pipeline.

$\mathbf{L_I}$	$\mathbf{L_E}$	NIQE↓	BRISQUE↓	NIMA↑
		3.908	22.919	4.599
✓		**3.706**	23.479	4.460
	✓	4.333	15.464	**4.890**
✓	✓	3.753	**11.762**	4.856

Table 3: Contribution of specific data synthesis components.

Model	NIQE↓	BRISQUE↓	NIMA↑
FDU	4.504	21.152	4.511
PDU	3.796	14.011	4.546
G+L	3.894	14.712	4.736
L+G	4.087	16.226	4.632
L+L	3.928	18.312	4.673
Reverse	3.838	17.094	4.633
IDU(Ours)	**3.753**	**11.762**	**4.856**

Table 4: Analysis of the Dehazing Unit.

Analysis of the Dehazing Unit. We evaluate the IDU by replacing it in IADNet with the following alternatives: 1) FDU, 2) PDU, 3) G+L (global features for $\mathbf{L_I}$), 4) L+G (global features for $\mathbf{L_I}$), 5) L+L (same scale local features for both terms), 6) Reverse (finer scale for $\mathbf{L_E}$), and 7) Ours (finer scale for $\mathbf{L_I}$). Results shown in Table 4 demonstrate that our IDU consistently outperforms other methods, effectively capturing dehazing features. FDU and PDU are feature dehazing units based on the ASM. Options 3) and 4) illustrate the impact of modifying only one item in ASM, while our approach proves the effectiveness of the proposed IASM from another perspective. Additionally, the comparison of scales—5) same scale, 6) finer $\mathbf{L_E}$, and 7) finer $\mathbf{L_I}$—supports our physical explanation that $\mathbf{L_I}$ should indeed have a finer scale than $\mathbf{L_E}$.

Conclusion

In this paper, we introduce an effective Physics Embedded Illumination Estimation (PEIE) method for real-world adaptive dehazing. Our proposed Illumination-Adaptive Scattering Model (IASM) accurately captures the illumination conditions of hazy scenes, addressing the limitations of traditional ASM. By leveraging the robust modeling capability of IASM, our data synthesis pipeline generates highly realistic paired data, significantly enhancing the quality of dehazing results. Furthermore, our Illumination-Adaptive Dehazing Unit (IDU) efficiently extracts dehazing features within the latent space, serving as a cornerstone of our dehazing network. Extensive experiments validate that PEIE outperforms state-of-the-art dehazing methods in the real world.

Acknowledgments

This work was partially supported by the National Natural Science Foundation of China (No.62122011, U21A20514), the "Pioneer" and "Leading Goose" R&D Program of Zhejiang (Grant No.2023C01030), and the Key R&D Program Project of Hangzhou (Grant No.2024SZD1A03).

References

Berman, D.; Treibitz, T.; and Avidan, S. 2016. Non-Local Image Dehazing. In *CVPR*.

Bui, T. M.; and Kim, W. 2018. Single Image Dehazing Using Color Ellipsoid Prior. *TIP*.

Cai, B.; Xu, X.; Jia, K.; Qing, C.; and Tao, D. 2016. DehazeNet: An End-to-End System for Single Image Haze Removal. *TIP*.

Cai, Y.; Bian, H.; Lin, J.; Wang, H.; Timofte, R.; and Zhang, Y. 2023. Retinexformer: One-Stage Retinex-Based Transformer for Low-Light Image Enhancement. In *ICCV*.

Chen, Z.; Wang, Y.; Yang, Y.; and Liu, D. 2021. PSD: Principled Synthetic-to-Real Dehazing Guided by Physical Priors. In *CVPR*.

Choi, L. K.; You, J.; and Bovik, A. C. 2015. Referenceless Prediction of Perceptual Fog Density and Perceptual Image Defogging. *TIP*.

Dong, H.; Pan, J.; Xiang, L.; Hu, Z.; Zhang, X.; Wang, F.; and Yang, M.-H. 2020. Multi-Scale Boosted Dehazing Network With Dense Feature Fusion. In *CVPR*.

Dong, J.; and Pan, J. 2020. Physics-Based Feature Dehazing Networks. In *ECCV*.

Fan, J.; Weng, J.; Wang, K.; Yang, Y.; Qian, J.; Li, J.; and Yang, J. 2024. Driving-Video Dehazing with Non-Aligned Regularization for Safety Assistance. In *CVPR*.

Fattal, R. 2015. Dehazing Using Color-Lines. *TOG*.

Gong, R.; Dai, D.; Chen, Y.; Li, W.; Paudel, D. P.; and Van Gool, L. 2021. Analogical Image Translation for Fog Generation. In *AAAI*.

Guo, C.-L.; Yan, Q.; Anwar, S.; Cong, R.; Ren, W.; and Li, C. 2022. Image Dehazing Transformer with Transmission-Aware 3d Position Embedding. In *CVPR*.

He, K.; Sun, J.; and Tang, X. 2011. Single Image Haze Removal Using Dark Channel Prior. *TPAMI*.

Hu, H.-M.; Guo, Q.; Zheng, J.; Wang, H.; and Li, B. 2019. Single Image Defogging Based on Illumination Decomposition for Visual Maritime Surveillance. *TIP*.

Hu, H.-M.; Zhang, H.; Zhao, Z.; Li, B.; and Zheng, J. 2020. Adaptive Single Image Dehazing Using Joint Local-Global Illumination Adjustment. *TMM*.

Ju, M.; Ding, C.; Ren, W.; Yang, Y.; Zhang, D.; and Guo, Y. J. 2021. IDE: Image Dehazing and Exposure Using an Enhanced Atmospheric Scattering Model. *TIP*.

Li, B.; Lin, Y.; Bai, J.; Hu, P.; Lv, J.; and Peng, X. 2022. Unsupervised Neural Rendering for Image Hazing. *TIP*.

Li, B.; Peng, X.; Wang, Z.; Xu, J.; and Feng, D. 2017. AOD-Net: All-In-One Dehazing Network. In *ICCV*.

Li, B.; Ren, W.; Fu, D.; Tao, D.; Feng, D.; Zeng, W.; and Wang, Z. 2019. Benchmarking Single-Image Dehazing and Beyond. *TIP*.

Li, C.; Zhou, H.; Liu, Y.; Yang, C.; Xie, Y.; Li, Z.; and Zhu, L. 2023. Detection-Friendly Dehazing: Object Detection in Real-World Hazy Scenes. *TPAMI*.

Li, L.; Dong, Y.; Ren, W.; Pan, J.; Gao, C.; Sang, N.; and Yang, M.-H. 2020. Semi-Supervised Image Dehazing. *TIP*.

Li, Y.; Tan, R. T.; and Brown, M. S. 2015. Nighttime Haze Removal with Glow and Multiple Light Colors. In *ICCV*.

Liao, L.; Chen, W.; Zhang, Z.; Xiao, J.; Yang, Y.; Lin, C.-W.; and Satoh, S. 2023. Only a Few Classes Confusing: Pixel-Wise Candidate Labels Disambiguation for Foggy Scene Understanding. In *AAAI*.

Ling, P.; Chen, H.; Tan, X.; Jin, Y.; and Chen, E. 2023. Single Image Dehazing Using Saturation Line Prior. *TIP*.

Liu, Y.; Zhu, L.; Pei, S.; Fu, H.; Qin, J.; Zhang, Q.; Wan, L.; and Feng, W. 2021. From Synthetic to Real: Image Dehazing Collaborating with Unlabeled Real Data. In *ACM MM*.

Meng, G.; Wang, Y.; Duan, J.; Xiang, S.; and Pan, C. 2013. Efficient Image Dehazing with Boundary Constraint and Contextual Regularization. In *ICCV*.

Mittal, A.; Moorthy, A. K.; and Bovik, A. C. 2012. No-Reference Image Quality Assessment in the Spatial Domain. *TIP*.

Mittal, A.; Soundararajan, R.; and Bovik, A. C. 2013. Making a "Completely Blind" Image Quality Analyzer. *IEEE Signal Processing Letters*.

Narasimhan, S.; and Nayar, S. 2002. Vision and the Atmosphere. *IJCV*.

Narasimhan, S.; and Nayar, S. 2003. Contrast Restoration of Weather Degraded Images. *TPAMI*.

Qin, X.; Wang, Z.; Bai, Y.; Xie, X.; and Jia, H. 2020. FFA-Net: Feature Fusion Attention Network for Single Image Dehazing. In *AAAI*.

Qiu, Y.; Zhang, K.; Wang, C.; Luo, W.; Li, H.; and Jin, Z. 2023. MB-TaylorFormer: Multi-Branch Efficient Transformer Expanded by Taylor Formula for Image Dehazing. In *ICCV*.

Ren, W.; Liu, S.; Zhang, H.; Pan, J.; Cao, X.; and Yang, M.-H. 2016. Single Image Dehazing via Multi-scale Convolutional Neural Networks. In *ECCV*.

Shao, Y.; Li, L.; Ren, W.; Gao, C.; and Sang, N. 2020. Domain Adaptation for Image Dehazing. In *CVPR*.

Song, Y.; He, Z.; Qian, H.; and Du, X. 2023. Vision Transformers for Single Image Dehazing. *TIP*.

Talebi, H.; and Milanfar, P. 2018. NIMA: Neural Image Assessment. *TIP*.

Wang, C.; Pan, J.; Lin, W.; Dong, J.; Wang, W.; and Wu, X.-M. 2024a. Selfpromer: Self-Prompt Dehazing Transformers with Depth-Consistency. In *AAAI*.

Wang, H.; Yue, Z.; Xie, Q.; Zhao, Q.; Zheng, Y.; and Meng, D. 2021a. From Rain Generation to Rain Removal. In *CVPR*.

Wang, X.; Xie, L.; Dong, C.; and Shan, Y. 2021b. Real-ESRGAN: Training Real-World Blind Super-Resolution With Pure Synthetic Data. In *ICCVW*.

Wang, Y.; Yan, X.; Wang, F. L.; Xie, H.; Yang, W.; Zhang, X.-P.; Qin, J.; and Wei, M. 2024b. UCL-Dehaze: Toward Real-World Image Dehazing via Unsupervised Contrastive Learning. *TIP*.

Wang, Z.; Zhao, H.; Peng, J.; Yao, L.; and Zhao, K. 2024c. ODCR: Orthogonal Decoupling Contrastive Regularization for Unpaired Image Dehazing. In *CVPR*.

Wu, R.; Duan, Z.; Guo, C.; Chai, Z.; and Li, C. 2023. RIDCP: Revitalizing Real Image Dehazing via High-Quality Codebook Priors. In *CVPR*.

Yang, L.; Kang, B.; Huang, Z.; Xu, X.; Feng, J.; and Zhao, H. 2024. Depth Anything: Unleashing the Power of Large-Scale Unlabeled Data. In *CVPR*.

Yang, X.; Xu, Z.; and Luo, J. 2018. Towards Perceptual Image Dehazing by Physics-Based Disentanglement and Adversarial Training. In *AAAI*.

Yang, Y.; Wang, C.; Liu, R.; Zhang, L.; Guo, X.; and Tao, D. 2022. Self-Augmented Unpaired Image Dehazing via Density and Depth Decomposition. In *CVPR*.

Zhang, H.; and Patel, V. M. 2018. Densely Connected Pyramid Dehazing Network. In *CVPR*.

Zhang, K.; Liang, J.; Van Gool, L.; and Timofte, R. 2021. Designing a Practical Degradation Model for Deep Blind Image Super-Resolution. In *ICCV*.

Zhang, Y.; Zhou, S.; and Li, H. 2024. Depth Information Assisted Collaborative Mutual Promotion Network for Single Image Dehazing. In *CVPR*.

Zhao, H.; Shi, J.; Qi, X.; Wang, X.; and Jia, J. 2017. Pyramid Scene Parsing Network. In *CVPR*.

Zheng, Y.; Zhan, J.; He, S.; Dong, J.; and Du, Y. 2023. Curricular Contrastive Regularization for Physics-Aware Single Image Dehazing. In *CVPR*.

Zhou, H.; Chang, Y.; Yan, W.; and Yan, L. 2023. Unsupervised Cumulative Domain Adaptation for Foggy Scene Optical Flow. In *CVPR*.